Energy Reports 12 (2024) 1566–1579

Contents lists available at ScienceDirect

Energy Reports

journal homepage: www.elsevier.com/locate/egyr

Research paper

Performance test of a heliostat field integrated PVT solar collector using organic phase change material and carbon black additives☆

Pabitro Prosad Mondal, Md. Atikur Rahman, Md. Shahriar Mohtasim, Md. Golam Kibria *, Ashik Hasan, Md. Sanowar Hossain, Pronob Das, Md. Forhad Ibne Al Imran, Mohd. Rafiqul A. Beg

Department of Mechanical Engineering, Rajshahi University of Engineering & Technology, Rajshahi 6204, Bangladesh

ARTICLE INFO

Keywords:
Heliostat field concentrator
Stearic acid
Carbon black
PVT collector

ABSTRACT

The rising global awareness of environmental issues has brought about a rise in the adoption of green energy throughout our daily activities in recent decades. The radiation from the sun is utilized for thermal heating, electrical generation, and agriculture by Phase change materials (PCM) integrated PVT collector. However, the lower concentration ratio of solar radiation on flat plate collectors and the lower thermal conductivity of PCMs are the major drawbacks. In this present study, a Heliostat field concentrator was designed to integrate with a hybrid photovoltaic thermal (PVT) collector for the increase of the solar irradiance, and carbon black additives incorporated stearic acid (SA) were used in the underneath PVT collector to enhance the thermal conductivity of SA as well as the thermal efficiency of the system. The performance tests were carried out for both SA with carbon black and SA without carbon black additives for varying water flow rates of 0.0025 kg/s, 0.0035 kg/s, 0.0045 kg/s, and 0.0055 kg/s. The efficiency of the PV panels ranged from 10 % to 13 %. The maximum thermal efficiency was found to be 46.56 % when using SA with carbon black for the water flow rate of 0.0035 kg/s whereas the maximum thermal efficiency was 45.45 % in the case of SA without carbon black for that water flow rate. Especially contrasted with the other flow rates throughout the investigation, the average thermal efficiency increases by 6.83 % for the flow rate of 0.0035 kg/s after integrating carbon black with PCM. The experimented results showed the outlet temperature of water in the range of 50 °C-59 °C throughout the day which is sufficient for domestic hot water applications.

1. Introduction

In the current era marked by escalating energy demands and heightened environmental apprehensions, exploring alternatives to non-renewable and environmentally detrimental fossil fuels is imperative. Despite this urgency, the world predominantly relies on traditional, nonrenewable energy sources such as coal, gas, and petroleum. The extensive consumption of these resources raises concerns about their eventual depletion. Solar thermal technology emerges as a viable substitute for these conventional energy sources. Solar energy, an abundant and inexhaustible resource, possesses a colossal potential to meet global energy needs sustainably (Kalidasan et al., 2020). The sun's power intercepted by the Earth far exceeds current energy consumption rates. Approximately 35 % of solar radiation is reflected in space, with 47 % reaching the Earth. Regions worldwide can generate significant solar electricity, making solar energy economically competitive with fossil fuels. Moreover, solar energy stands out for its environmental cleanliness and global availability. Harnessing even a fraction of the total solar energy potential can align with climate change recommendations. A substantial increase in renewable energy usage could stabilize fuel prices, alleviate market pressures, and reduce carbon emissions. Despite ongoing efforts, only 20 % of solar resources are currently utilized, emphasizing the need for maximizing solar energy utilization by 2025 (Al-Mohamad, 2004).

In residential settings, solar thermal energy has proven to be both effective and economical for heating water. This involves harnessing energy during periods of abundant sunlight to preheat water for later use during high-demand periods. However, a notable challenge lies in the

☆ A full research paper submitted for publication in "Energy Reports"

* Corresponding author.
E-mail address: kibria@me.ruet.ac.bd (Md.G. Kibria).

https://doi.org/10.1016/j.egyr.2024.07.031
Received 26 February 2024; Received in revised form 27 June 2024; Accepted 13 July 2024

mismatch between hot water demand and energy availability (Liu et al., 2006). Thermal energy storage (TES) systems offer a solution to align energy supply with usage demand. These systems, often including hot water storage tanks, encounter spatial constraints in smaller living spaces, a challenge mitigated by phase change material (PCM) storage systems (Kibria et al., 2024a).

PCMs, also known as latent heat energy storage systems, store energy during the melting phase and release it during solidification (Anika et al., 2024). The solar collector is a device that captures sunlight, transferring the collected heat to the fluid in contact with it. A typical flat-plate collector consists of a metal box with a top cover (glazing), an absorber plate, and insulation to minimize heat loss (Liu et al., 2006). While flat plate solar water collectors (FPSWCs) are widely used in solar energy applications, challenges arise from the intermittent nature of solar radiation and variable hot water demand intervals. To address this, latent heat storage (LHS) devices with PCMs enhance the thermal performance of solar water heaters by storing excess solar energy and releasing it when sunlight is unavailable. Solid-liquid PCMs are commonly employed in solar water collectors, undergoing phase transition to absorb/release heat. Solar irradiance raises the PCM temperature to its melting point during the day, and the PCM continues absorbing heat until its entire mass transitions from solid to liquid. Upon sunset, the liquid PCM solidifies, releasing stored heat (Kabeel et al., 2017).

Solar energy can be used directly in a variety of thermal applications like heating water, heating air, drying, distillation, cooking, air-conditioning, power generation and other purposes. Each system needs a critical temperature for its operation. In order to obtain the required temperature, flat-plate collectors are commonly used. Some attention has also been given to using concentrator collectors, specifically Heliostat Field Concentrator. Heliostat field Concentrator can achieve higher temperatures compared to flat-plate. For the efficient operation of a system, a consistent supply of the required temperature is important. However, solar energy is not constant throughout the day; it increases as the sun rises higher in the sky in the middle of the day and decreases in the afternoon as the sun lowers its position (Kanka et al., 2024). Normally, solar collectors are straight, facing south. In this case, the required temperature is obtained in the middle of the day. To obtain the required temperature for a longer period of time, the solar energy needs to be captured efficiently in the morning and afternoon. In this study, we designed a Photovoltaic-Thermal (PVT) with Heliostat Field Concentrator with PCM to capture maximum energy.

Kibria et.al (Kibria et al., 2024b). examined the effect of Al_2O_3-ZnO NPs on paraffin wax as a hybrid PCM /PVT system for energy, exergy and exergoeconomic analysis. This hybrid system improved the thermal efficiency and overall efficiency by 17.32 % and 13.82 % respectively. Besides, the electrical efficiency was found to be increased by 34.84 % with improved exergy efficiency. The exergoeconomic analysis showed 16.67 % less cost with 2.1 years of payback time. Bhutto et.al (Bhutto et al., 2024). investigated the silver-graphene nanoparticles-based Lauric Acid phase change material for the PVT system to produce a thermoelectric generator. The thermal conductivity of lauric acid was increased by 57 % due to the incorporation of 3.5 wt% of Silver-graphene NPs whereas the latent heat enhancement was 8 % which resulted in the improvement of thermal efficiency. Additionally, the chemical and thermal stability was observed good after 500 thermal cycles for PCM LAG-3.5. Almeshaal et.al (Almeshaal and Altohamy, 2024). conducted an experimental analysis of a Cu_2O nanofluid-incorporated paraffin wax PVT collector to enhance thermal and electrical efficiency. This study exhibited an overall thermal efficiency of 82.1 % and a 37.7 % improvement in electrical efficiency compared to conventional PV.

In the literature, Table 1 provides information on the performance of PVT systems using a PCM and TiO_2 nanofluid. The highest maximum power increase is obtained with 1.0 wt% TiO_2 nanofluid (Mohd Razali et al., 2020). The maximum electrical and thermal efficiency for

Table 1
Summarized literature review of recent works on PVT.

Strategy Employed	Findings	Limitations	Year	Ref.
The paper proposes a novel framework for PVT systems using a PCM. Experiment-based research was conducted in Malaysian weather conditions.	PV performance (both electrical and thermal) increased with the use of PCMs. Maximum electrical and thermal efficiency for PVT-PCM were 15.32 % and 86.19 %, respectively.	PCM was used to enhance the electrical and thermal efficiency of solar PV systems. However, the performance of PV was not evaluated.	2023	(Hossain et al., 2023a)
Utilization of cooling nano fluid circulation system with micro fin tube. Encapsulation of nano PCM with nanoparticles.	PVT had an electrical efficiency of 9.6 %. PVT-PCM had a thermal efficiency of 77.5 %.		2023	(Bassam et al., 2023)
Three-dimensional modeling using Comsol 5.4 software and Matlab. Analysis of hybrid PVT collector based on (P3HT: PCBM).	Maximum temperature of the PVT collector: 110.09Â°C. Higher thermal efficiency (85.77 %) and lower electrical efficiency (6.57 %) compared to monocrystalline silicon PVT collector.	Limited raw materials and competition with other uses. The toxicity of materials, particularly CdTe, makes recycling complex and costly.	2022	Haloui et al., (2022)
Hybrid PVT solar energy collector with integrated PCM. Combination of air-based and water-based conditions for building heat demand.	The overall efficiency of the system is 39.4 %. Energy-saving efficiency of the system is 64.2 %.	The paper does not compare the PVT-PCM system with other existing solar energy collection technologies or discuss its limitations in comparison to alternative approaches.	2022	(Li et al., 2022)
Design and analysis of a novel solar cooling system. Utilization of environmentally friendly refrigerants to reduce global warming issues.	Solar cooling efficiency increased by 33.1 %. Refrigeration cycle performance coefficient (COP) improved by 8.23 %.	It does not discuss potential challenges or drawbacks associated with the implementation or, practicality of the system.	2022	(Zarei et al., 2022)
Thermal modelling using MATLAB. Analysis of PVT-TEC air collector for the month of June.	The average thermal gain of the PVT-TEC air collector increased from 15.28 W to 49.51 W when the transmissivity of the PV module glass varied from 0.3 to 0.95. The electrical efficiency of the air collector varied from 14.66 % to	The study does not consider the long-term effects or durability of the PV module glass with varying transmissivity, which could be important for practical applications.	2022	Singh et al., (2022)

(continued on next page)

Table 1 (*continued*)

Strategy Employed	Findings	Limitations	Year	Ref.
	13.89 % and the electrical.			
Investigation of various PVT-PCM solar collector designs.	Electrical efficiency improvement: usually less than 20 %. Thermal efficiency improvement: usually up to 70 %.	Lack of research on the economy and environmental evaluation. Need for improvements in collector designs and optimization.	2021	(Nižetić et al., 2021)
A system with PCM embedded in porous metal. Water is used as a heat transfer fluid (HTF) with a constant mass flow rate of 30 kg/hr.	Enhanced melting fraction of PCM by 6 % and 8 % for PVT-PCM/Cu and PVT-PCM/Al systems. Overall efficiency increased by 10.62 % and 8.80 % for PVT-PCM/Cu and PVT-PCM/Al systems.	The study only focuses on the numerical analysis of the PVT-PCM system with PCM embedded in highly conductive porous material, without experimental validation.	2021	Pawar et al., (2021)
The authors presented an experimental investigation that improves the efficiency of a PVT water collector with and without titania (TiO_2) nanofluid using a spiral absorber as a coolant.	The highest maximum power increase is obtained with 1.0 wt% TiO_2 nanofluid. The generated power increases with the addition of solar radiation.	The paper does not provide information on the sample size or the duration of the experimental investigation	2020	(Mohd Razali et al., 2020)
Development of a novel PVT collector. Comparison and analysis of thermal and electrical efficiencies of different PVT configurations.	Electrical and thermal efficiencies of PVT collectors are 15.4 % and 73 %. Lower PV modules and higher fluid operating temperatures were achieved with the new PVT configuration.	The paper does not discuss the cost-effectiveness or economic feasibility of the novel PVT collector design.	2020	(Rejeb et al., 2020)
Concentrating PVT dual-fluid solar collector. Analytical expressions derived from energy balance equations for each component.	Incorporating two fluids increases thermal and electrical efficiencies. Total thermal and electrical efficiencies achieved are 67 % and 13.02 % respectively.	-The paper does not mention any limitations in terms of the generalizability or scalability of the findings to larger-scale applications.	2020	(Baljit et al., 2020)

PVT-PCM systems were 15.32 % and 86.19 %, respectively (Hossain et al., 2023a). The electrical efficiency of PVT with PCM was 9.6 %, while the thermal efficiency was 77.5 % (Bassam et al., 2023). The paper also discusses the utilization of cooling nano fluid circulation systems with micro fin tubes and the encapsulation of nano PCM with nanoparticles. The authors presented an experimental investigation that improved the efficiency of a PVT water collector with and without TiO_2 nanofluid using a spiral absorber as a coolant (Cuenca et al., 2010).

The utilization of various fillers to enhance the thermal conductivity of organic PCMs is acknowledged, emphasizing the need to minimize filler content to preserve the high energy density of PCMs. Despite the known benefits of PCMs in solar thermal storage applications, there is limited research on the incorporation of carbon black additives to enhance the energy absorptivity and thermal conductivity of PCMs as well as the thermal efficiency of PVT collectors. Additionally, as per the authors' knowledge, there is no research on integrating a Heliostat Field Concentrator to such a carbon black-PCM-based PVT collector to increase the concentration ratio of solar radiation for both electrical and thermal performance enhancement. This study's primary objectives are to design a Heliostat Field Concentrator integrating a PVT collector for enhancement of the solar irradiance of the PVT collector. Besides, this study focuses on improving the thermal efficiency of hybrid PVT collectors by integrating stearic acid as a phase change material with carbon black additives. The authors aim to demonstrate the design of solar energy systems encompassing both thermal and PV components. To enhance thermal efficiency, the research endeavours to integrate PCM into the PVT system. Performance assessment involves an energy analysis of both electrical and thermal aspects. Notably, the PVT-PCM system, as indicated by the findings, exhibits lower cell temperatures compared to alternative systems.

2. Materials and methods

In this experiment, a Heliostat field concentrator with a PVT collector is utilized. Thermal and electrical energy are both provided by PVT collectors. The PV panel is attached to the side of the flat plate collector in this hybrid setup. Fig. 1 shows the sectional and top view of a PVT solar collector for the experimental setup.

2.1. PCM selection

Choosing a PCM for a latent heat energy storage system (LHESS) depends on the intended application. Considerations include the PCM's melting point within the desired temperature range for effective heat storage and release, high latent heat of fusion for optimal storage density, elevated specific heat to incorporate sensible heat storage, and enhanced thermal conductivity. Additional factors encompass minimal volume changes during phase transition, absence of sub-cooling during solidification, chemical stability, non-toxic and non-flammable characteristics, reasonable cost, and ready accessibility (Zhang and Fang, 2006). In the context of a solar domestic hot water system, careful PCM selection is crucial to ensure desired water temperatures and address safety concerns like potential PCM leakage into the building's water supply.

Organic PCMs are well suited for solar energy storage because of their small freezing and melting temperature range, and their congruent melting. Most organic PCMs are also readily available, relatively cheap and nontoxic. Organic PCMs have been widely studied in solar energy storage, but not as combined energy storage and radiation absorption media. Table 2 shows the thermo-physical properties of stearic acid

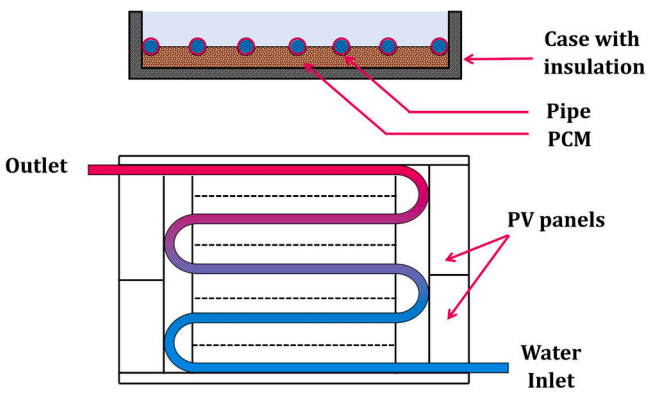

Fig. 1. Sectional and top view of a PVT solar collector.

Table 2
Thermo-physical properties of SA.

Property	Values
Appearance and phase	White and solid
Melting temperature	52 ℃
Density	847–965 kg/m^3
Thermal conductivity	0.29 W/m. K
Latent heat of fusion	198.8 KJ/kg
Specific heat	1.59 KJ/kg K
Cubical expansion coefficients	810×10^{-6} /K

Table 3
Properties and composition of carbon black (Pierson, 1993).

Composition	Amount (%)	Properties	Amount
Hydrogen	0.05–1.0	Surface Area	25–150 m^2/g
Nitrogen	0.02–0.09	Particle Size	10–500 mm
Oxygen	2.5–7.0	Oil absorption	0.5–1.5 cm^3/g
Sulfur	0.01–0.03	-	-
CO_2	0.1–1.5	-	-
CO	0.2–4.0	-	-
Carbon	Balance	-	-

(SA). This temperature range permits it to successfully preserve and release thermal energy while being within the functional range of most solar collectors. Furthermore, the large energy storage capacity maximizes the quantity of solar energy that may be preserved and utilized later, improving the efficiency of solar collectors compared to other PCMs like paraffin wax, salt hydrates and eutectic mixtures. Repetitive cycles of solidification and melting are unable to readily break down SA due to its long-term chemical stability. Moreover, SA can create a hydrophobic layer that aids in lowering the buildup of water and dust on solar collector surfaces. Over time, this characteristic helps to keep the collectors efficient and clean (Yuan et al., 2022; Mohtasim and Das, 2024).

Fig. 2 shows the classification of phase change material. The slow charging and discharging rates of PCMs, owing to their inherently low thermal conductivity, necessitate heat transfer enhancements (Agyenim, 2016). Utilizing carbon nanofillers, such as graphite nanoparticles, proves effective in improving both thermal conductivity and energy storage properties without significantly impacting phase change enthalpies or temperatures. The extent of thermal conductivity enhancements depends on nanofiller geometry, with graphite nanoparticles exhibiting a notable 164 % relative enhancement at 5 wt% loading. Additionally, the introduction of ethylene glycol (EG) in PCM composites reduces melting times by 16 % and 32 % for 4 wt% and 10 wt% EG, respectively, due to heightened heat transfer from increased thermal conductivity (Sari and Kaygusuz, 2001). Notably, a paraffin/expanded graphite composite PCM, as devised by Zhang & Fang, exhibits substantial thermal storage capacity, improved thermal conductivity, and phase change integrity without liquid leakage (Zhang and Fang, 2006). Table 3 shows the properties and composition of carbon black (Pierson, 1993).

2.2. Analytical analysis

2.2.1. Determining the collector area

The temperature of the water at the inlet, $T_{in} = 30$ ℃, and the temperature of the water exit, $T_{out} = 50$ ℃. (minimum temperature for use of domestic hot water system). If the water flow rate is $\dot{m} = 8.57 kg/hr$, and the efficiency is taken into account is, $\eta = 35\%$. The specific heat of water is taken as, $Cp = 4187 J/kg.K$. Total heat transfer $\dot{q} = 698 W/m^2$ (source: weather Directorate) (Mohtasim and Das, 2024),

$$\dot{q} = \quad m \quad Cp \quad (T_{out} - T_{in}) \tag{1}$$

Heat incident on the collector $= (A_C \times 698 \times 0.35) = 200$W. Therefore, the collector area is obtained as, $A_C = 0.81\ m^2$.

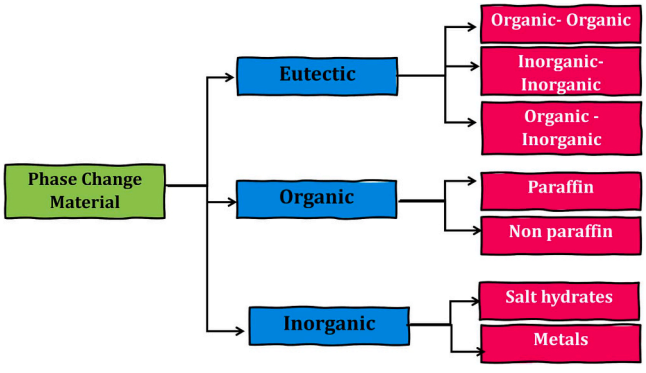

Fig. 2. Classification of phase change material.

2.2.2. Thermal resistance

By taking into account the surface temperature of the receiver, thermal conduction is obtained throughout the glass and then transferred into the heat transfer fluid via convection heat transfer. Next, it might be carried by convection towards the rear sidewalls of the receiver and through the walls by conductions. The thermal resistances are calculated by the following equations (Qenawy et al., 2023).

$$R_{cond,absorber\ plate} = \frac{t}{L \times w \times k_{plate}} \tag{2}$$

$$R_{cond,copper\ pipe} = \frac{\ln \frac{r_0}{r_i}}{2\pi \times L \times k_{plate}} \tag{3}$$

$$R_{conv,inlet\ water\ flow} = \frac{1}{h_i \times A_i} \tag{4}$$

$$R_{cond,PCM} = \frac{\ln \frac{r_0}{r_i}}{2\pi \times L \times k_{pcm}} \tag{5}$$

Where, $h_i = \frac{N_u \times k}{D}$.

N_u is the Nusselt number, D is the half of the passage thickness. T is thickness of absorber plate, W is width of contact between pipe and plate, K is the thermal conductivity h_i is Heat transfer coefficient, r_0 and r_i are the outer and inner radius of copper pipe and R is the thermal resistance.

2.2.3. Determining the mass of PCM

Amount of energy release, $Q = m \times L$. Where, m is the mass of substance in kg, L is the latent heat of fusion in KJ/kg (Siala and Elayeb, 2001). PCM to dissipate heat in 2 hr. are, $Q = m\ s\Delta T \times t$, which is equal to 0.93 kWh. Now, $m = Q/L = 0.93 \times 3600 / 198.8 = 16.50 kg$.

2.2.4. Mass of carbon black

Mey (Mey, 2016) added carbon black with SA in a composition of 0.01 % to 6 wt%. Therefore, authors are intended to use 1 wt% of carbon black with SA to ensure the optimum performance. So, the mass of the stearic acid is 16.50 kg and the mass of the carbon black becomes 165 gm.

2.2.5. Heliostat field layout design

The main idea of the heliostat field layout design is to locate the receiver and the mirrors in a given land area. Once the column space and line space between the mirrors are determined, the number of the mirrors of each row and column can easily be figured out. Thus, a field layout is generated to calculate the corresponding annual optical efficiency and the ground coverage. Table 4 lists the decision variables and their description for cornfield pattern, where H_t is the height of the aim point of the receiver tower, l_m is the length of the heliostat, W_m is the

Table 4
Decision variable for cornfield pattern.

Decision variables	Description	Search range
R_o	The distance between the receiver and the first row.	$[0.70H_t, 1.5H_t]$
dx	Column space	$[DM, 2l_m]$
dy	Row space	$[DM, W_m/\sin(h_r)]$

Table 5
The dimensions of the designed heliostat field concentrator.

Parameters	Dimensions
Height of the tower	72"
Length of the mirror	14"
Width of the mirror	14"
Radius of the 1st row of heliostat	50.4"
Radius of the 2nd row of heliostat	76"
Radius of the 3rd row of heliostat	102"
Height of the 1st row of heliostat	18"
Height of the 2nd row of heliostat	27"
Height of the 3rd row of heliostat	39"

width of the heliostat h_r is the elevation angle of the reflected vectors of the heliostats.

Where, H_t is height of the receiver tower, l_m is length of the heliostat, width of the heliostat is denoted as W_m, h_r is elevation angle of the reflected vectors of the heliostats. The lower bound of the search range of column space and line space between mirrors is determined by the safety distance (Siala and Elayeb, 2001). Fig. 3 shows the top and side view for no blocking. The layout of radial stagger pattern is shown in Fig. 4.

$$DM = \sqrt{l_m^2 + W_m^2} + ds \tag{6}$$

The upper bound of the decision variables (Cerecedo et al., 2013) are considered as such that $L_1 = 2l_m$. That means Mirror B will not block Mirror A at any time. The length of L_2 can also be determined by $L_2 = W_m = \sin(h_r)$. For the lower bound of the decision variables, the minimum radius of the heliostats should ensure that it does not happen that adjacent heliostats have mechanical collisions.

$$\Delta R_{\min} = R_{m+1,\min} - R_{\min} = DM \times \cos 30^o \times \cos\beta_L \tag{7}$$

Where, β_L is the tilt angle of the field. The maximum radius should be determined according the principle that there is no blocking between the heliostats (Koca et al., 2008) as shown in Fig. 5. The calculation is as follows:

$$Z_m = R_m \times \tan\beta_L + H_h \tag{8}$$

$$d = \sqrt{R_m{}^2 + (H_c - Z_m)^2} \tag{9}$$

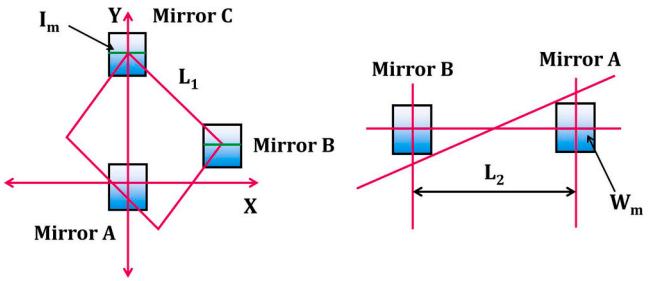

Fig. 3. Top and side view for no blocking.

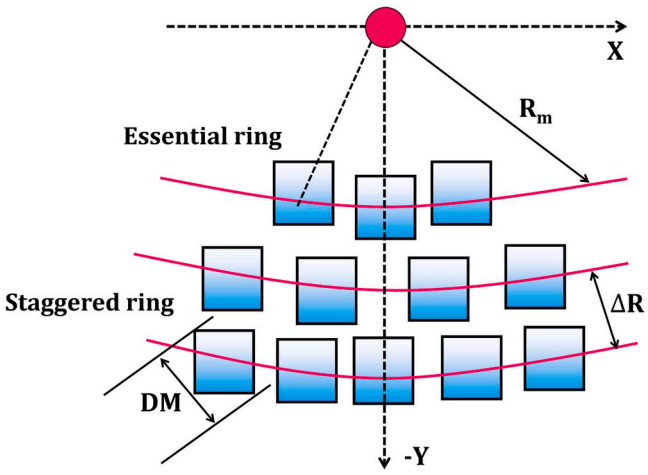

Fig. 4. Layout of radial stagger pattern.

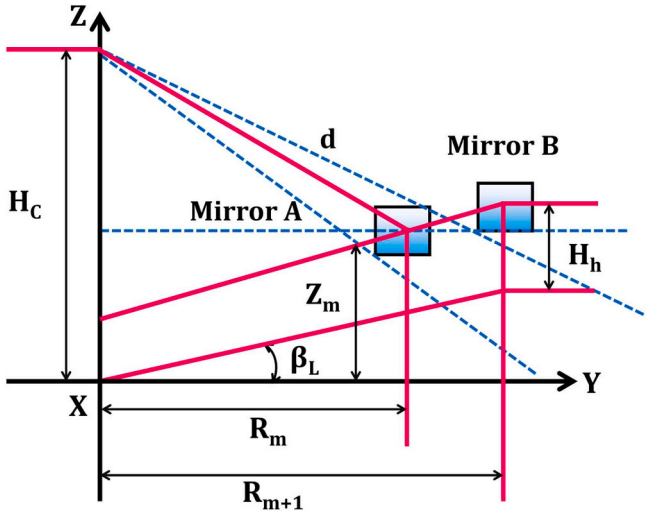

Fig. 5. Radius for no blocking.

$$\gamma = \sin^{-1}\left(\frac{DM}{2d}\right) + \sin^{-1}\left(\frac{R_m}{d}\right) - \beta_L \tag{10}$$

$$\Delta R_{\min} = R_{m+1,\min} - R_{\min} = DM\ cos\beta_L / \cos\gamma \tag{11}$$

So, the radius of each ring can be expressed as follows,

$$R_{m+1} = R_m + \Delta R_{\min} + R_{coeff}(\Delta R_{\max} - \Delta R_{\min}); 0 < R_{coeff} < 1 \tag{12}$$

2.2.6. Heliostat field concentrator design

The lower bound of the search range of column space and line space between mirrors is determined as follows (Koca et al., 2008),

$$DM = \sqrt{l_m^2 + W_m^2} + ds = \sqrt{(14^2 + 14^2)} + 5 = 24.80'' \quad \approx 25''$$

Height of the first heliostat,

$$Z_1 = R_m \quad \tan\beta_L + H_u = 0.70 \times 72 \times \tan 20^o + 0 = 18''$$

$$\Delta R_{\min} = R_{m+1,\min} - R_{\min} = \mathrm{DM} \times \cos 30^O \quad \times \cos\beta_L$$
$$= 25 \times \cos 30^O \quad \times 20^O = \quad 20.35''$$

$$d = \sqrt{R_m{}^2 + (H_c - Z_m)^2} = \sqrt{50.4^2 + (72 - 18)^2} = 73.87''$$

$$\gamma = \sin^{-1}\left(\frac{DM}{2d}\right) + \sin^{-1}\left(\frac{R_m}{d}\right) - \beta_L = \sin^{-1}\frac{25}{2\times 73.87} + \sin^{-1}\frac{50.4}{73.87} - 20 = 33^{\circ}$$

$$\Delta R_{\min} = R_{m+1,\min} - R_{\min} = DM\ cos\beta_L/\cos\gamma = (25\times\cos 20^{O})/\cos 33^{O} = 28''$$

Now, the radius of the (m+1) th row, $R_{\ 2} = 50.4 + 20.35 + 0.7(28 - 20.35) = 76''$

Height of the 2nd row heliostat, $Z_m = R_m \times \tan\beta_L + H_h = 76\tan 20^{0} + 0 = 27''$

2.2.7. Electrical and thermal efficiency

Energy collected by the system can be calculated by Hotter-Whillier-Bliss equation (El-Sebaii et al., 2009). The useful energy gain of the system is the sum of PCM is used to heat and water carried heat from the system. Total useful energy of the system Q_u and useful energy of water Q_w are given by,

$$Q_u = A_c \times F_R \quad [S - U_L(Ti - Ta)] \tag{13}$$

$$Q_w = \quad m \quad c_p \quad (To - Ti) \tag{14}$$

Instantaneous thermal efficiency, η_t of the flat plate collector and electrical efficiency of the PV panel, η_e can be determined by Darbari et al (Darbari and Rashidi, 2021). as follows,

$$\eta_t = F_R(\propto T) - F_R U_L \frac{(T_i - T_a)}{G} \tag{15}$$

$$F_R = \quad \frac{m \quad C_p(T_o - T_a)}{A_c[S - U_l(T_i - T_a)]} \tag{16}$$

$$\eta_e = \frac{P}{GA_{pv}} \tag{17}$$

$$S = \quad G(\propto\tau) \tag{18}$$

Where, A_c is the collector area, G is the solar irradiance, τ is the transmittance of any cover plate, $\propto$ is the absorptance of the collector, T_a is the ambient temperature, T_i is the inlet temperature, T_o is the outlet temperature, U_l is the overall heat loss coefficient, m is the mass flow rate of fluid through the collector, P is the output power, A_{pv} is the area of the solar panel.

2.2.8. Uncertainty analysis

Uncertainty analysis is conducted to verify the precision of the experimental findings, and the calculation of the uncertainty analysis for the experimental results can be performed using equation (Divya et al., 2022),

$$V_A = [(\frac{\partial A}{\partial u_1}v_1)^2 + (\frac{\partial A}{\partial u_2}v_2)^2 + \ldots(\frac{\partial A}{\partial u_n}v_n)^2]^{.5} \tag{19}$$

In this equation, the uncertainty, denoted as V_A, is associated with the independent variable functions are represented by A. The uncertainties $v_1, \ldots, v_n$ correspond to $u_1, \ldots, u_n$. The thermal and electrical performance, considering the uncertainties, can be derived using the aforementioned equation.

3. Experimental setup

The experimental work is conducted at the Heat Engine roof, RUET under district Rajshahi, Bangladesh. The latitude 24.3745°N, longitude 88.6042°E. Solar energy available in the location is 6.39 $kWh/m^2.day$. The wind speed in the location is taken as 2 m/s. Fig. 6 shows the schematic of Heliostat Field Concentrator with the experimental layout.

The experimental setup is fabricated by locally available materials. The experimental setup is mainly aiming to test the performance of the collector with an integrated heliostat field concentrator. The effects on mass flow rates are also considered. The model with carbon black and the model without carbon black was not tested at the same time. Firstly, the required amount of SA was added to the underneath of a leakage-free container of the PVT collector and the experiments were conducted for the water flow rate of 0.0025 kg/s (05/06/2023), 0.0035 kg/s (06/06/2023), 0.0045 kg/s (12/06/2023), and 0.0055 kg/s (15/06/2023). Then, the carbon black additives were mixed stoichiometrically with SA. The required amount of SA was taken to a magnetic stirrer maintaining a constant temperature of 60 °C for melting down. After complete melting, the liquid stearic acid was continuously stirred for 10 minutes. The stoichiometric ratio of carbon black was gradually added to the liquid phase to prevent clumping and uniform distribution while continuously stirred for 30 minutes. The liquid phase was then transferred to an ultrasonicator and sonicated for 30 minutes keeping a constant temperature of 60 °C for homogeneous distribution of carbon black into the

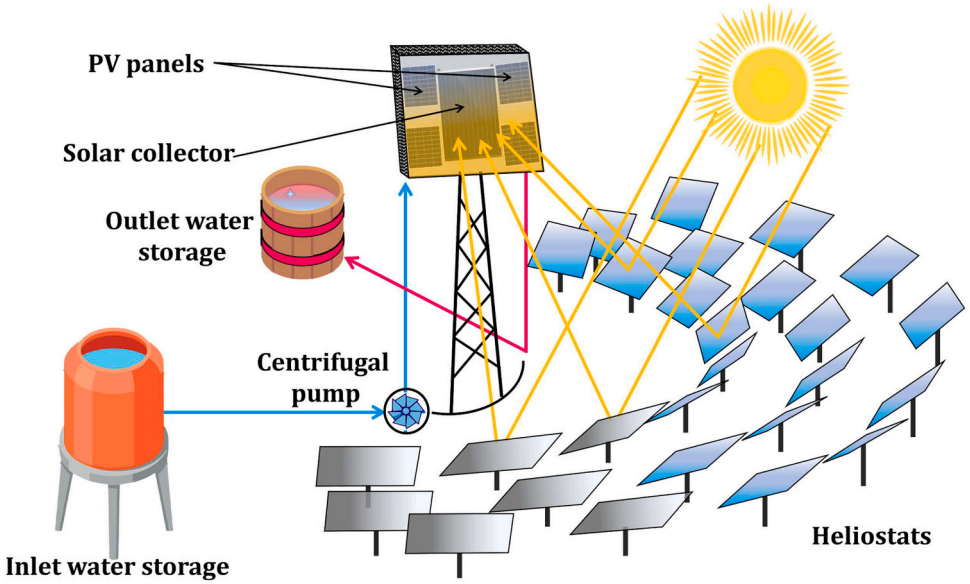

Fig. 6. Schematic of heliostat field concentrator.

SA matrix by breaking down the agglomeration of carbon black. After complete mixing the carbon black-SA liquid phase was poured into the leakage-free copper container that was attached underneath the water-containing copper tube by brazing into the PVT collector. The performance of the PVT collector was then tested for varying water flow rates the water flow rates of 0.0025 kg/s (26/06/2023), 0.0035 kg/s (28/06/2023), 0.0045 kg/s (02/07/2023), and 0.0055 kg/s (05/07/2023). The experiments were done throughout the day from 10.00 am to 6.00 pm and the temperature variations, the heat transfer rate and performance were analyzed. Figs. 7 and 8 show the photograph of the heliostat field concentrator with the experimental setup.

The length and width of the used PVT collector are 1 m and 0.80 m respectively. Four PV panels from TRI-G Solar are attached to the collector. Each of the panels has maximum power, open circuit voltage and short circuit current of 5 W, 21.5 V and 0.32 A respectively. A 2.54 cm diameter and 1 m length of copper tube is used for passing the water through the collector. A storage tank with a capacity of 16.5 kg PCM is attested to the collector. The flow rate of the water is controlled by an available small flow control centrifugal pump.

To increase the concentration ratio, the PVT system is integrated with a heliostat field concentrator. In the designed heliostat field, there are 20 Heliostats made of plane mirrors of having (14×14) square inch area each. The height of the central tower is 72" from the ground. The total number of Heliostat are placed at three different rows. Where the first row consists of 5 Heliostat having radius from the central tower of 50.4" with the height of 18". The second row consists of 6 Heliostat having radius from the central tower of 76" with the height of 27" and the first row consists of 5 Heliostat having a radius from the central tower of 102" with the height of 39".

After setting up the total system water is supplied by a flow control Pump into the inlet pipe of the collector. The sun ray is directly reflected from different heliostats and concentrated into the PVT collector. This increases the concentration ratio. The heat is absorbed by the PCM and the cold water. The hot water is obtained from the outlet pipe. Electric power is obtained from the photovoltaic cell. As there is no automatic tracking system, the position of the collector and the heliostat needs to be manually controlled.

3.1. Experimental methodology

Firstly, the collector was placed in a sunny area towards the sun. Then the reflector was set in such a way that the sun rays concentrated on the absorber plate. After that, the water was followed by using a flow control centrifugal pump. After every 1 hour later ambient temperature, and outlet temperature were measured with the help of a thermometer. At the same time, the solar intensity was measured with the help of a pyranometer. For photovoltaic efficiency current and voltage were measured with the help of an Ammeter and voltmeter. Again, the position of the reflector was changed manually. The above procedure was repeated from 10 A.M. to 06 P.M. with an interval of 1 hour.

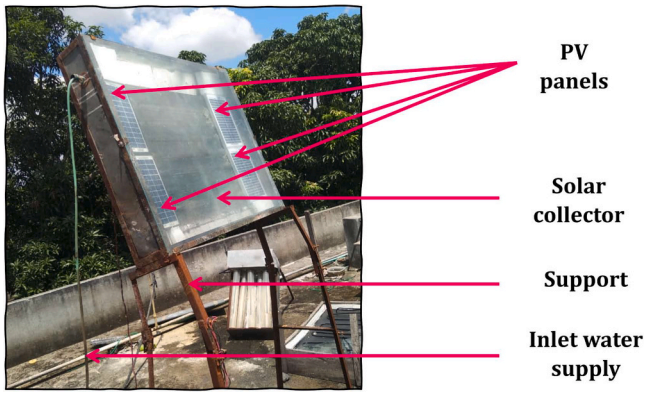

Fig. 8. Photograph of the PVT Collector.

4. Result and discussion

The performance of the PVT collector includes the output temperature, thermal efficiency and the electrical efficiency of PV panels. The performance was carried out for the water flow rate of 0.0025 kg/s, 0.0035 kg/s. 0.0045 kg/s and 0.0055 kg/s. For each water flow rate, the experiments were done for PCM with carbon black and without carbon black. Different graphs for ambient temperature, output temperature and solar intensity against the time of the day at different water flow rates for PCM with carbon black and without carbon black are plotted in this section.

From Figs. 9 and 10, it is clear that the output temperature gradually increased from 10 AM to 1 PM then it decreased gradually to 6 PM for using PCM with carbon black and without carbon black at the water flow rate of 0.0025 kg/s. The output temperature was always greater when carbon black with PCM was used. The maximum output temperature was 58 °C and 59 °C corresponding to the maximum solar intensity of 805 W/m^2 and 820 W/m^2 for using PCM without carbon black additives and with carbon black additives respectively.

From Figs. 11 and 12, it is evident that while employing PCM with

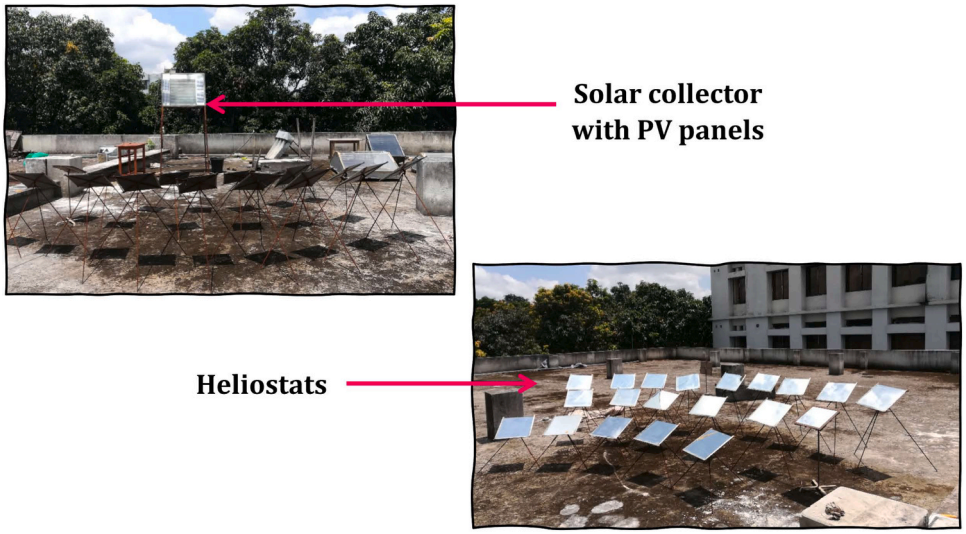

Fig. 7. Photograph of the heliostat field concentrator with experimental setup.

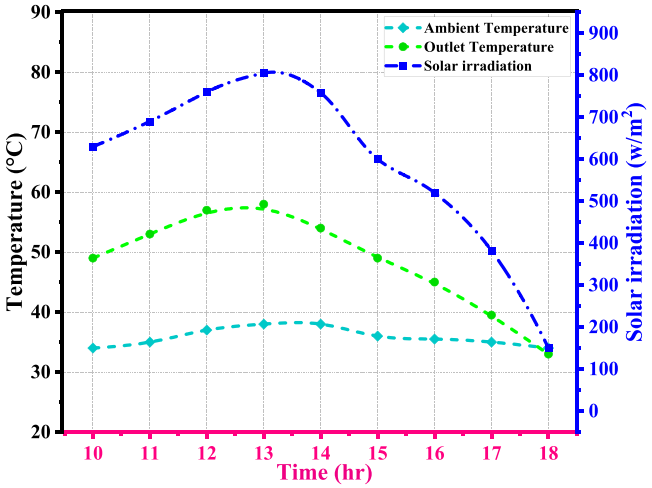

Fig. 9. Ambient temperature, output temperature and solar intensity against time for water flow rate 0.0025 kg/s (PCM without carbon black).

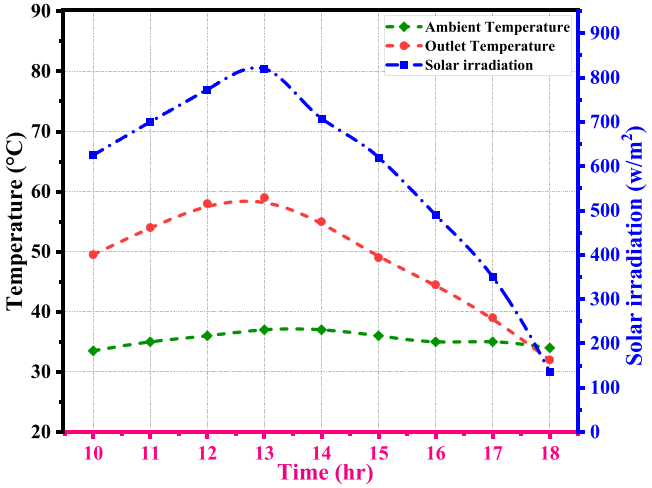

Fig. 10. Ambient temperature, output temperature and solar intensity against time for flow rate 0.0025 kg/s (PCM with carbon black).

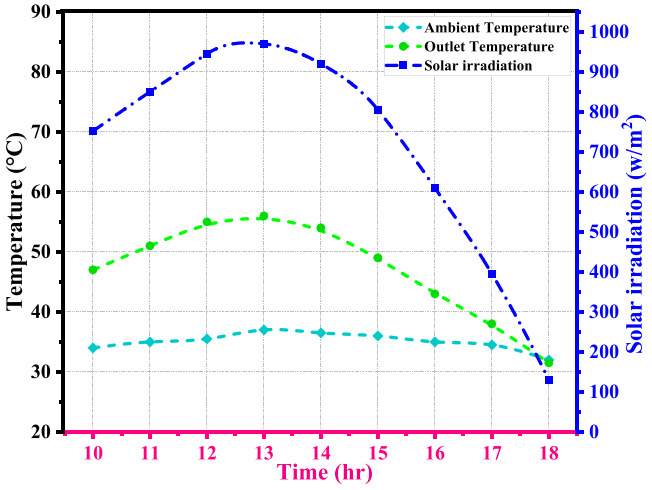

Fig. 11. Ambient temperature, output temperature and solar intensity against time for flow rate 0.0035 kg/s (PCM without carbon black).

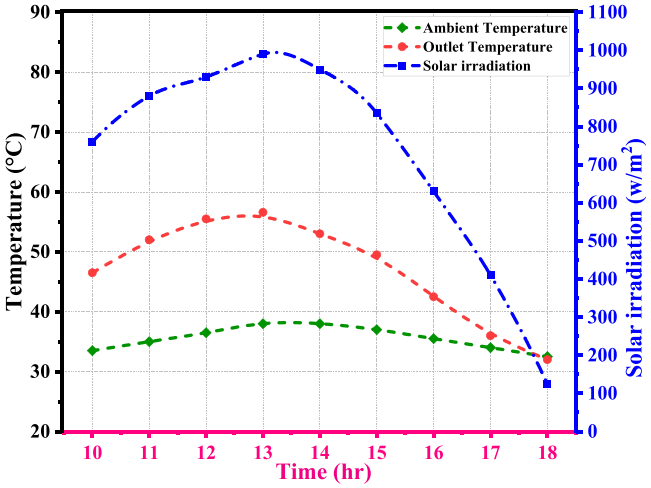

Fig. 12. Ambient temperature, output temperature and solar intensity against time for flow rate 0.0035 kg/s (PCM with carbon black).

carbon black and without carbon black at the water flow rate of 0.0035 kg/s, which is equivalent to the prior water flow rate of 0.0025 kg/s, the output temperature gradually climbed from 10 AM to 1 PM and then declined gradually until 6 PM. The output temperature was always greater when carbon black with PCM was used. The maximum output temperature was 56 °C and 56.5 °C corresponding to the maximum solar intensity of 970 W/m^2 and 990 W/m^2 for using PCM without carbon black and with carbon black additives respectively. The water output temperature was somewhat less at the flow rate of 0.0035 kg/s because of the increase in the flow rate the previous.

The output temperature for both the PCM with and without carbon black at the water flow rate of 0.0045 kg/s, which corresponds to the same as the preceding water flow rates, steadily climbed from 10 AM to 1 PM and subsequently fell to 6 PM, as shown in Figs. 13 and 14. When PCM and carbon black were combined, the output temperature was always higher. The maximum output temperature was 51 °C and 52.5 °C corresponding to the maximum solar intensity of 1050 W/m^2 and 1080 W/m^2 for using PCM without carbon black and with carbon black additives respectively. The water output temperature was somewhat less at the flow rate of 0.0045 kg/s because of the increase in the flow rate than the previous.

From the aforementioned two Figs. 15 and 16, it is evident that while employing PCM with carbon black and without carbon black at the

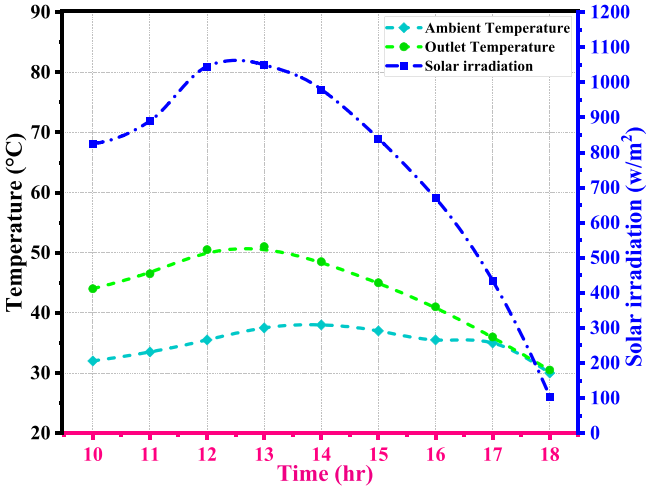

Fig. 13. Ambient temperature, output temperature and solar intensity against time for flow rate 0.0045 kg/s (PCM without carbon black).

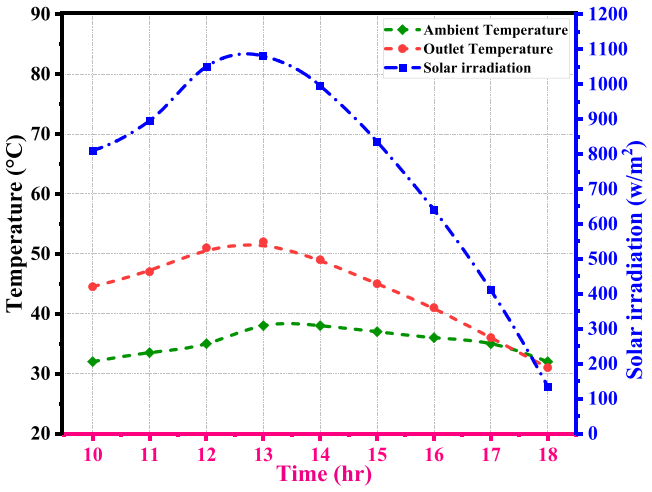

Fig. 14. Ambient temperature, output temperature and solar intensity against time for flow rate 0.0045 kg/s (PCM with carbon black).

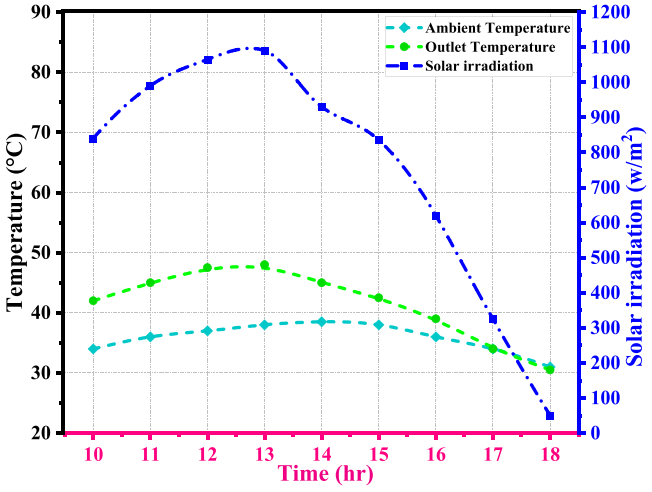

Fig. 15. Ambient temperature, output temperature and solar intensity against time for flow rate 0.0055 kg/s (PCM without carbon black).

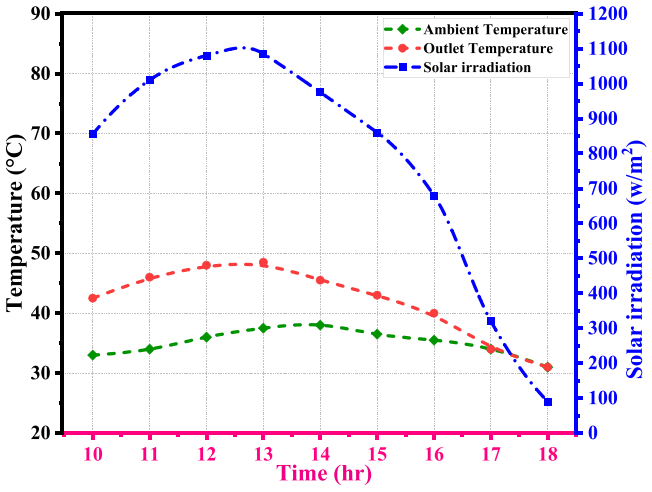

Fig. 16. Ambient temperature, output temperature and solar intensity against time for flow rate 0.0055 kg/s (PCM with carbon black).

water flow rate of 0.0055 kg/s, which corresponds to the same as the earlier water flow rates, the output temperature gradually climbed from 10 AM to 1 PM and then declined gradually to 6 PM. When carbon black and PCM were utilized together, the output temperature was always higher. The maximum output temperature was 48 °C and 48.5 °C corresponding to the maximum solar intensity of 1090 W/m^2 and 1085 W/m^2 for using PCM without carbon black and with carbon black additives respectively. The water output temperature was somewhat less at the flow rate of 0.0055 kg/s because of the increase in the flow rate than the previous.

From Figs. 17 and 18, it is clear that the thermal efficiency gradually increased from 10 AM to 1 PM then it decreased gradually to 6 PM for using PCM with carbon black and without carbon black at the water flow rate of 0.0025 kg/s. The thermal efficiency was always greater when carbon black with PCM was used. The thermal efficiency varies from 37 % to 43 % for using PCM without carbon black and 39–45 % for using PCM with Carbon Black additives. However, there is no difference in electrical efficiency between 9.5 % and 12 % when utilizing PCM with or without carbon black. The electrical efficiency was found to decline when the solar panel's temperature climbed.

The thermal efficiency for both the PCM with and without carbon black at the water flow rate of 0.0035 kg/s, which is the same as the previous water flow rate of 0.0025 kg/s, steadily increased from 10 AM to 1 PM and then decreased to 6 PM, as can be seen from the Figs. 19 and 20**.** Using carbon black with PCM consistently resulted in higher thermal efficiency. The range of thermal efficiency for PCM without carbon black additives is 39–45.50 %, while for PCM with carbon black additives, it is 40–46.56 %. Compared to the prior water flow rate of 0.0025 kg/s, the thermal efficiency was marginally higher. But there is no effect on electrical efficiency of using PCM with or without carbon black and it varies from 10 % to 12.50 %. It is observed that the electrical efficiency of PV decreased with increasing the temperature of the solar panel as the previous water flow rate.

From Figs. 21 and 22, it is evident that while employing PCM with carbon black and without carbon black at the water flow rate of 0.0045 kg/s, which corresponds to the same as the previous water flow rates, the thermal efficiency gradually improved from 10 AM to 1 PM and then fell gradually until 6 PM. When carbon black and PCM were utilized together, the thermal efficiency was always higher. When using PCM without carbon black, the thermal efficiency ranges from 38 % to 44.50 %, but when using PCM with carbon black additions, the range is 39–45.50 %. The flow rate may have an impact on the efficiency of the heat transfer method. At higher flow rates, the fluid may not have enough residence time to absorb sufficient heat, leading to a lower outlet

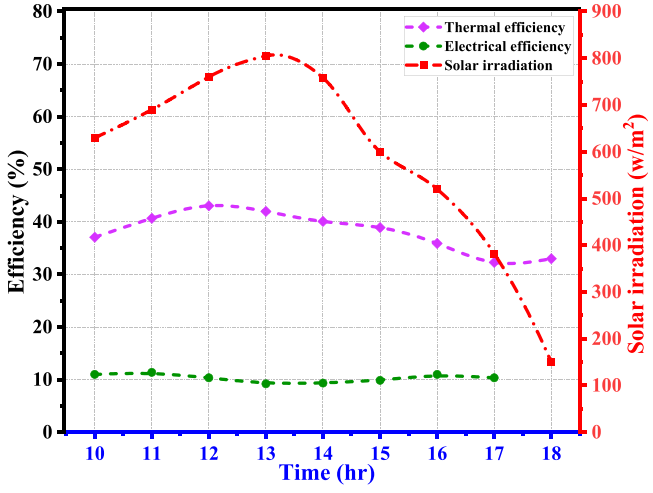

Fig. 17. Thermal efficiency, photovoltaic efficiency and the solar intensity against time for water flow rate 0.0025 kg/s (PCM without carbon black).

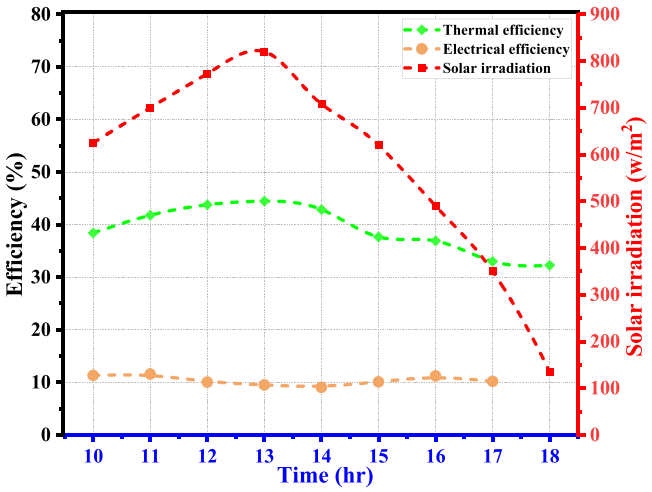

Fig. 18. Thermal efficiency, photovoltaic efficiency and the solar intensity against time for water flow rate 0.0025 kg/s (PCM with carbon black).

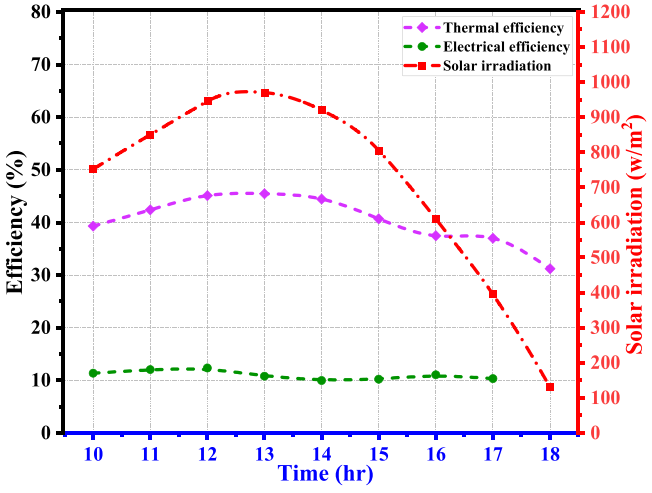

Fig. 19. Thermal efficiency, photovoltaic efficiency and the solar intensity against time for water flow rate 0.0035 kg/s (PCM without carbon black).

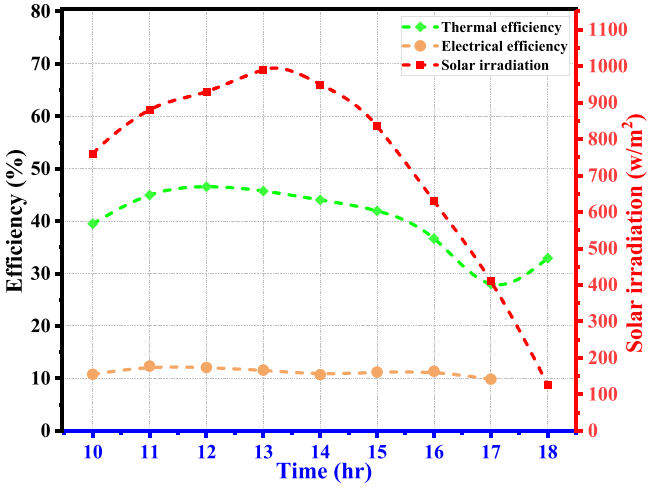

Fig. 20. Thermal efficiency, photovoltaic efficiency and the solar intensity against time for water flow rate 0.0035 kg/s (PCM with carbon black).

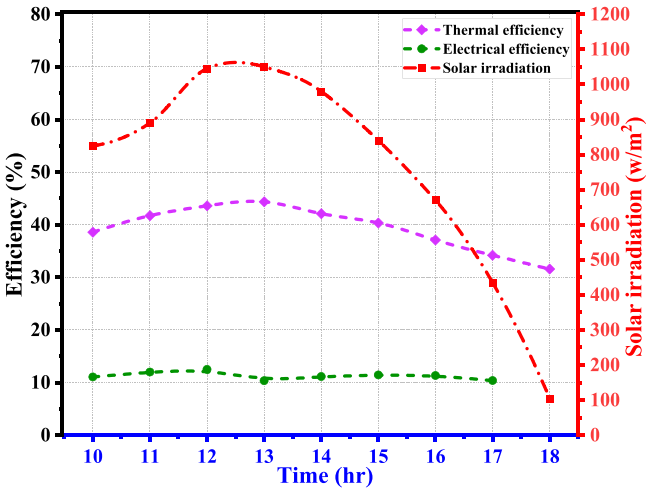

Fig. 21. Thermal efficiency, photovoltaic efficiency and the solar intensity against time for water flow rate 0.0045 kg/s (PCM without carbon black).

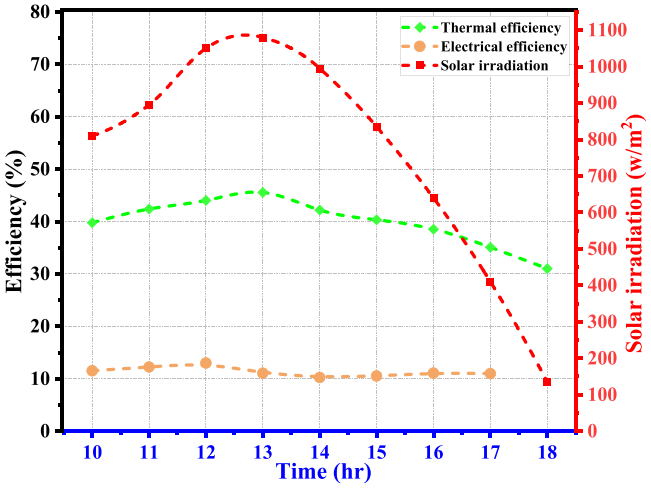

Fig. 22. Thermal efficiency, photovoltaic efficiency and the solar intensity against time for water flow rate 0.0045 kg/s (PCM with carbon black).

temperature and thus reduced thermal efficiency. The thermal efficiency was less compared to the flow rate of 0.0035 kg/s but slightly higher than the prior water flow rate of 0.0025 kg/s. However, employing PCM with or without carbon black has little influence on electrical efficiency, which ranges from 10.50 % to 13 %. It has been noted that when the temperature of the solar panel rose relative to the prior water flow rate, the electrical efficiency of the PV dropped.

From Figs. 23 and 24, when employing PCM with carbon black and without carbon black at the water flow rate of 0.0055 kg/s, which is equivalent to the previous water flow rates, it is evident that the thermal efficiency steadily grew from 10 AM to 1 PM and subsequently declined to 6 PM. The thermal efficiency was always greater when carbon black with PCM was used. The thermal efficiency varies from 36 % to 42.50 % for using PCM without carbon black and 37–44 % for using PCM with Carbon Black additives respectively. Since the fluid was moving more rapidly, there was a lower overall heat transfer rate, which led to poorer thermal efficiency. From the four different flows, the maximum thermal efficiency was found at 0.0035 kg/s. The electrical efficiency of PCM, however, varies from 10 % to 12.50 % and is unaffected by the presence or absence of carbon black.

Fig. 25 shows the electrical output power of PV panel over time taken 1 hour interval from 10 AM to 5 PM. The curves clearly indicate that the output powers are firstly increasing. The decreasing behavior of the

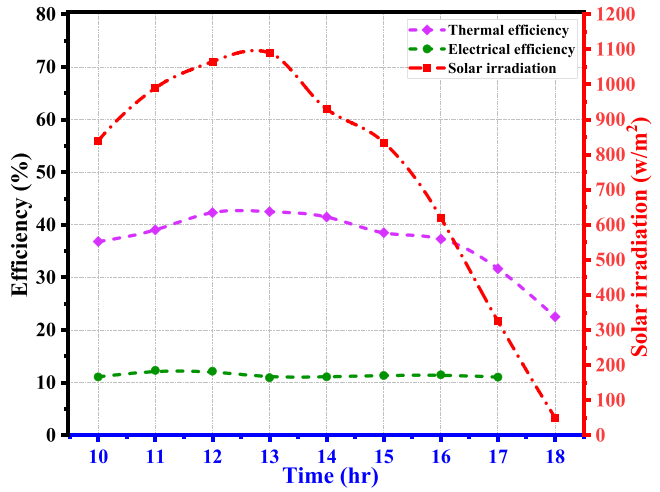

Fig. 23. Thermal efficiency, photovoltaic efficiency and the solar intensity against time for water flow rate 0.0055 kg/s (PCM without carbon black).

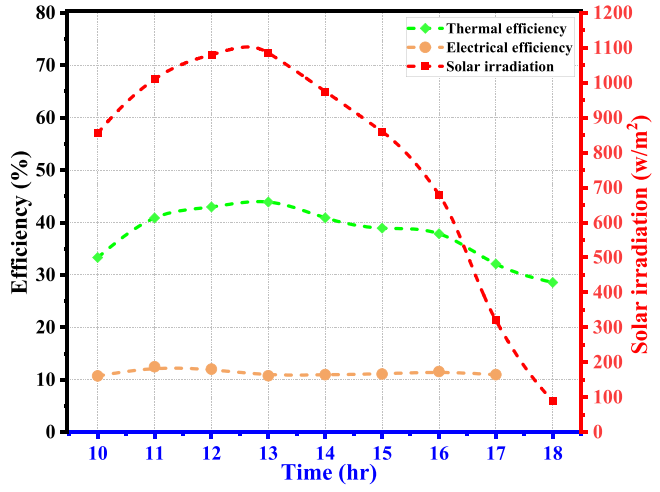

Fig. 24. Thermal efficiency, photovoltaic efficiency and the solar intensity against time for water flow rate 0.0055 kg/s (PCM with carbon black).

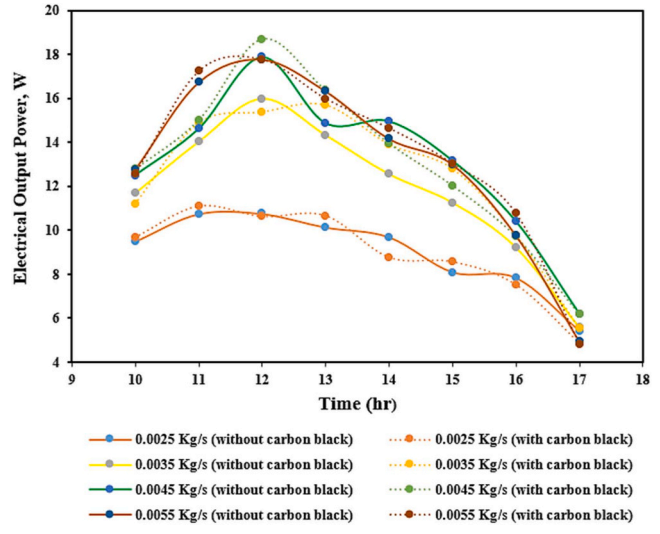

Fig. 25. Variation of Electrical Output Power using PCM with carbon black and without carbon black for the water flow rate of 0.0025 kg/s, 0.0035 kg/s 0.0045 kg/s and 0.0055 kg/s.

output powers are observed from midday. This variation between increasing and decreasing was due to the solar irradiation variation throughout the day. Furthermore, the electrical output power of the PVT-PCM system with carbon black is somewhat higher than the system without carbon black. The carbon black increased the thermal conductivity of the PCM that increased the heat transfer rate resulting in the reduction of cell temperature. However, the maximum electrical output power was found to be 17.77 W at the water flow rate of 0.0045 Kg/s for the system PVT-PCM with carbon black. The increased water flow rate reduced the cell temperature by transferring more heat from the system. Which ultimately increased the electrical output temperature of the PV cell as well as the electrical efficiency.

The thermal efficiency of PCM with and without carbon black was compared (Fig. 26 (a) and (b)) for water flow rates of 0.0025 kg/s, 0.0035 kg/s, 0.0045 kg/s, and 0.0055 kg/s. The heat transfer fluid maintains a good temperature gradient over the collector's length and improves convective heat transfer at its ideal flow rate. Heat transfer coefficients are higher in turbulent or transitional regimes of flow, which allows for more effective heat absorption from the solar absorber into the flowing fluid. At 0.0035 kg/s, thermal losses via radiation, convection, and conduction are reduced and heat is absorbed more evenly, resulting in an efficient heat transfer process free from notable

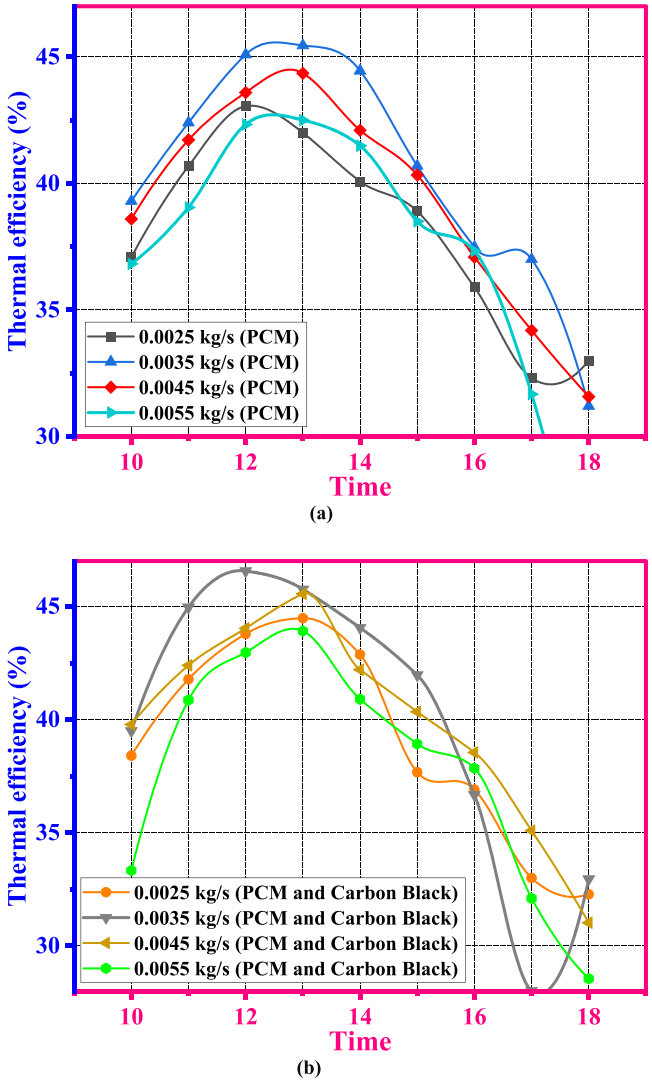

Fig. 26. The comparison of Thermal efficiency (%) using (a) without carbon black and (b) PCM with carbon black for water flow rate of 0.0025 kg/s, 0.0035 kg/s 0.0045 kg/s and 0.0055 kg/s.

temperature peaks or dips that could impair efficiency. While too low a flow rate can result in larger temperature gradients that enhance radiative losses, too high a flow rate can cause increased heat losses due to higher convective heat transfer coefficients on the external surfaces.

The results showed that the thermal efficiency of PCM with carbon black was higher than that of PCM devoid of carbon black. In both situations, the thermal efficiency grew from 0.0025 kg/s to 0.0035 kg/s at the flow rate. After reaching this flow rate, the efficiency decreased and the thermal efficiency became roughly stable at 0.0045 kg/s. The maximum thermal efficiency was found 46.56 % for using PCM with carbon black and 45.45 % for using without carbon black additives respectively when the flow rate was 0.0035 kg/s. So, 0.0035 kg/s is the desired water flow rate for the better performance of the PVT collector (Fig. 27).

Table 6 depicts the comparative performance analysis of the present study with similar technologies. System configurations, operating circumstances and weather conditions have a great influence on the performance of the PVT systems. Both thermal and electrical efficiency varies widely due to the design considerations, operating condition, location and environmental effects that make the comparison more challenging. However, our current study has analyzed a new system of integrating heliostat field in the PVT-PCM system and the effect of addition of carbon black into PCM.

5. Conclusion

A hybrid PVT collector (SA with carbon black) consisting of a flat plate collector and PV Panels integrated with a Heliostat field concentrator was designed and constructed for this study. In the designed heliostat field, there are 20 Heliostats made of plane mirrors having (14×14) square inch area each. The height of the central tower is 72" from the ground. The total number of Heliostat are placed in three different rows. Where the first row consists of 5 Heliostat having a radius from the central tower of 50.4" with a height of 18". The second row consists of 6 Heliostat having radius from the central tower of 76" with the height of 27" and the first row consists of 5 Heliostat having radius from the central tower of 102" with the height of 39". 1 wt% of carbon black was incorporated with SA having a mass of 16.5 kg to ensure the optimum performance of the solar collector with the mass flow rates of 0.0025 kg/s, 0.0035 kg/s, 0.0045 kg/s and 0.0055 kg/s. The results yield the following conclusions.

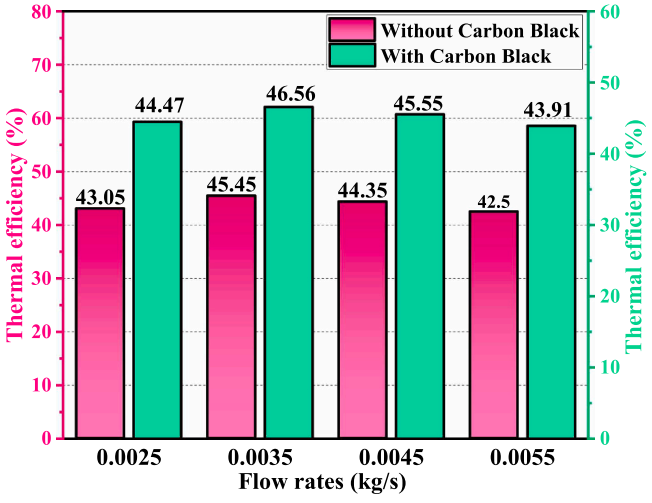

Fig. 27. Variation of maximum thermal efficiency using PCM with carbon black and without carbon black for the water flow rate of 0.0025 kg/s, 0.0035 kg/s 0.0045 kg/s and 0.0055 kg/s.

Table 6
Comparative analysis of performance with similar technology.

Technology	Thermal Efficiency	Electrical Efficiency	Ref.
Compound parabolic concentrators integrated PVT-PCM system	48.00 %	-	(Al Imam et al., 2023)
Compound parabolic concentrators mounted hybrid PVT- PCM (Paraffin wax) system	50.00 %	13.00 %	(Al Imam et al., 2016)
Nano-PCM twisted absorber tube PVT collector	79.40 %	9.46 %	(Al-Aasama et al., 2023)
Nanofluid coolant integrated Nano-PCM PVT system	58.00 %	14.00 %	(Al-Waeli et al., 2019)
Nano PCM-PV system	-	13.70 %	(Al-Waeli et al., 2020)
Nanofluid and Nano SiC-PCM based PVT system	72.00 %	13.70 %	(Al-Waeli et al., 2017)
Hybrid PVT-PCM system	65.00 %	12.75 %	(Fayaz et al., 2019)
Hybrid PVT-PCM system	64.50 %	14.00 %	(Alsaqoor et al., 2023)
Hybrid PVT-PCM system	86.19 %	11.51 %	(Hossain et al., 2023b)
PS-CNT foam incorporated PCM-PVT system	68.60 %	14.00 %	(Ahmadi et al., 2021)
Hybrid PVT-PCM system	70.34 %	8.16 %	(Yang et al., 2018)
Micro encapsulated PCM-PVT system	45.00 %–55.00 %	13.50 %	(Fu et al., 2021)
Present Study	**46.56 %**	**13.00 %**	

- The performance was tested in the proper way and the efficiency of the PV panels varied from 10 % to 13 %
- The thermal efficiency was varied from 39 % to 46.56 % for different water flow rates of 0.0025 kg/s,0.0035 kg/s,0.0045 kg/s and 0.0055 kg/s for using both PCM with carbon black and PCM without carbon black additives.
- When carbon black additives were not added to PCM, the highest thermal efficiency of the solar collector was attained at about 45.45 %; when they were added, it was 46.56 %, with a flow rate of 0.0035 kg/s, which is almost 2.45 % and 3.76 % higher than the flow rates of 0.0025 kg/s and 0.0055 kg/s respectively.
- Heat transfer coefficients are higher in turbulent or transitional regimes of flow, which allows for more effective heat absorption from the solar absorber into the flowing fluid. At 0.0035 kg/s, thermal losses via radiation, convection, and conduction are reduced and heat is absorbed more evenly, resulting in an efficient heat transfer process free from notable temperature peaks or dips that could impair efficiency.
- Compared to the other flow rates studied, the average thermal efficiency shows a significant increase of 6.83 % when integrating carbon black with PCM at a flow rate of 0.0035 kg/s.
- At 0.0035 kg/s water flow, PCM without carbon black reached 56 °C and 56.50 °C with carbon black. The PVT collector works best with 0.0035 kg/s of water flow.

6. Limitations and recommendations

Despite the design of a heliostat field integrated PVT collector, there was no sun tracking system of the heliostats to automatically reflect the solar radiation always on the PVT collector. A single PVT collector was unable to test the model with carbon black and the model without carbon black at the same time leading to difficulties in comparing real-time output from the PVT collector. Additionally, some researchers observed the significant inverse effect of increasing wind speed on the performance of PVT collectors throughout the day which was not taken into consideration during the performance test. As the experimental place (roof of the Heat Engine Lab, RUET, Rajshahi) was surrounded by

high-storied buildings and long trees, it was found to be the wind speed of 2 m/s in the morning and was almost the same throughout the day measured at 3-hour intervals. So, the authors thought that low wind speed and its slight variation would not be a significant parameter while several important parameters have been analyzed in this PVT system. However, it is strongly recommended to consider wind speed as a key parameter for further research as increasing wind speed decreases the thermal efficiency of PVT systems. An automatic sun tracking system is highly suggested for the system's convenience for both the PVT collector and the Heliostats. However, the incorporation of varying percentages of carbon black up to 3 % can be investigated in this PVT system for the enhancement of thermal conductivity and solar absorptivity of the SA. Additionally, high thermal conductive nanofillers such as Al_2O_3, MgO, and SiO_2 can be incorporated into the SA or similar PCM like Paraffin and lauric Acid for further research. As the efficiency of the PV panels decreases with increasing the temperature of the system, nanofluids such as TiO_2, Al_2O_3, and SiC-based cooling systems will be the further research to reduce the PV panel temperature at a reasonable level but not reducing the temperature of the flat plate collector. Besides, a system should be incorporated to transfer the reduced heat of solar panels to the PVT collector for the improvement of thermal efficiency. The economic and environmental evaluation can be considered to be an additional investigation to strengthen the values of electrical and thermal efficiency for the system in real-world applications.

CRediT authorship contribution statement

Pronob Das: Visualization. **Ashik Hasan:** Visualization, Formal analysis. **Md. Shahriar Mohtasim:** Writing – review & editing, Visualization, Validation. **Md.Golam Kibria:** Writing – review & editing, Formal analysis, Investigation. **Md. Sanowar Hossain:** Formal analysis. **Pabitro Prosad Mondal:** Writing – original draft, Methodology, Data curation, Conceptualization. **Md. Atikur Rahman:** Writing – original draft, Methodology, Investigation, Conceptualization. **Md. Forhad Ibne Al Imran:** Investigation. **Mohd. Rafiqul A. Beg:** Writing – review & editing, Supervision.

Declaration of Competing Interest

The authors declare that they have no known competing financial interests or personal relationships that could have appeared to influence the work reported in this paper.

Data availability

Data will be made available on request.

References

Agyenim, F., 2016. The use of enhanced heat transfer phase change materials (PCM) to improve the coefficient of performance (COP) of solar powered LiBr/H 2 O absorption cooling systems (Mar). Renew. Energy vol. 87, 229–239. https://doi.org/10.1016/j.renene.2015.10.012.

Ahmadi, R., Monadinia, F., Maleki, M., 2021. Passive/active photovoltaic-thermal (PVT) system implementing infiltrated phase change material (PCM) in PS-CNT foam (Apr). Sol. Energy Mater. Sol. Cells vol. 222, 110942. https://doi.org/10.1016/j.solmat.2020.110942.

Al Imam, M.F.I., Beg, R.A., Haque, M.J., Rahman, M.S., 2023. Effect of novel phase change material (PCM) encapsulated design on thermal performance of solar collector (Jun). Results Mater. vol. 18, 100388. https://doi.org/10.1016/j.rinma.2023.100388.

Al Imam, M.F.I., Beg, R.A., Rahman, M.S., Khan, M.Z.H., 2016. Performance of PVT solar collector with compound parabolic concentrator and phase change materials (Feb). Energy Build. vol. 113, 139–144. https://doi.org/10.1016/j.enbuild.2015.12.038.

Al-Aasama, A.B., Ibrahim, A., Syafiq, U., Sopian, K., Abdulsahib, B.M., Dayer, M., 2023. Enhancing the performance of water-based PVT collectors with nano-PCM and twisted absorber tubes (Aug). Int. J. Renew. Energy Dev. vol. 12 (5), 891–901. https://doi.org/10.14710/ijred.2023.54345.

Almeshaal, M.A., Altohamy, A.A., 2024. Experimental analysis of a photovoltaic thermal collector using phase change materials and copper oxide nanofluid (Jul). J. Energy Storage vol. 93, 112265. https://doi.org/10.1016/j.est.2024.112265.

Al-Mohamad, A., 2004. Efficiency improvements of photo-voltaic panels using a Sun-tracking system. Appl. Energy vol. 79 (3), 345–354. https://doi.org/10.1016/j.apenergy.2003.12.004.

Alsaqoor, S., Alqatamin, A., Alahmer, A., Nan, Z., Al-Husban, Y., Jouhara, H., 2023. The impact of phase change material on photovoltaic thermal (PVT) systems: a numerical study (May). Int. J. Thermofluids vol. 18, 100365. https://doi.org/10.1016/j.ijft.2023.100365.

Al-Waeli, A.H.A., et al., 2017. Evaluation of the nanofluid and nano-PCM based photovoltaic thermal (PVT) system: an experimental study (Nov). Energy Convers. Manag. vol. 151, 693–708. https://doi.org/10.1016/j.enconman.2017.09.032.

Al-Waeli, A.H.A., Chaichan, M.T., Sopian, K., Kazem, H.A., Mahood, H.B., Khadom, A.A., 2019. Modeling and experimental validation of a PVT system using nanofluid coolant and nano-PCM (Jan). Sol. Energy vol. 177, 178–191. https://doi.org/10.1016/j.solener.2018.11.016.

Al-Waeli, A.H.A., Sopian, K., Kazem, H.A., Chaichan, M.T., 2020. Evaluation of the electrical performance of a photovoltaic thermal system using nano-enhanced paraffin and nanofluids (Oct). Case Stud. Therm. Eng. vol. 21, 100678. https://doi.org/10.1016/j.csite.2020.100678.

Anika, U.A., Kibria, Md.G., Kanka, S.D., Mohtasim, Md.S., Paul, U.K., Das, B.K., 2024. Exergy, exergo-economic, environmental and sustainability analysis of pyramid solar still integrated hybrid nano-PCM, black sand, and sponge (May). Sol. Energy vol. 274, 112559. https://doi.org/10.1016/j.solener.2024.112559.

Baljit, S.S.S., Chan, H.Y., Zaidi, S.H., Sopian, K., 2020. Performance study of a dual-fluid photovoltaic thermal collector with reflection and refraction solar concentrators (Feb). Int. J. Low. -Carbon Technol. vol. 15 (1), 25–39. https://doi.org/10.1093/ijlct/ctz054.

Bassam, A.M., Sopian, K., Ibrahim, A., Fauzan, M.F., Al-Aasam, A.B., Abusaibaa, G.Y., 2023. Experimental analysis for the photovoltaic thermal collector (PVT) with nano PCM and micro-fins tube nanofluid (Jan). Case Stud. Therm. Eng. vol. 41, 102579. https://doi.org/10.1016/j.csite.2022.102579.

Bhutto, Y.A., Pandey, A.K., Saidur, R., Rathore, P.K.S., Samykano, M., 2024. Hybrid silver-graphene nanoparticles enhanced Lauric Acid phase change material for photovoltaic and thermoelectric generator applications: experimental and simulation analysis (Jul). J. Energy Storage vol. 93, 112320. https://doi.org/10.1016/j.est.2024.112320.

L.O.L. Cerecedo, N. Pitalua-Diaz, I. Salgado Transito, L.E. Velazquez Contreras, and C. Arancibia Bulnes, "Optical performance modeling of a solar tower heliostat field and estimation of receiver temperature," in *2013 IEEE International Autumn Meeting on Power Electronics and Computing (ROPEC)*, Nov. 2013, pp. 1–6. doi: 10.1109/ROPEC.2013.6702759.

Cuenca, L., Ortiz, A., Boza, A., 2010. Emerging trends in technological innovation. IFIP Adv. Inf. Commun. Technol. vol. 314 (February 2016), 24–31. https://doi.org/10.1007/978-3-642-11628-5.

Darbari, B., Rashidi, S., 2021. Thermal efficiency of flat plate thermosyphon solar water heater with nanofluids. J. Taiwan Inst. Chem. Eng. vol. 128, 276–287. https://doi.org/10.1016/j.jtice.2021.06.027.

Divya, S., et al., 2022. Analysing analyzing the performance of combined solar photovoltaic power system with phase change material. Energy Rep. vol. 8, 43–56. https://doi.org/10.1016/j.egyr.2022.06.109.

El-Sebaii, A.A., Al-Ghamdi, A.A., Al-Hazmi, F.S., Faidah, A.S., 2009. Thermal performance of a single basin solar still with PCM as a storage medium (Jul). Appl. Energy vol. 86 (7–8), 1187–1195. https://doi.org/10.1016/j.apenergy.2008.10.014.

Fayaz, H., Rahim, N.A., Hasanuzzaman, M., Nasrin, R., Rivai, A., 2019. Numerical and experimental investigation of the effect of operating conditions on performance of PVT and PVT-PCM (Dec). Renew. Energy vol. 143, 827–841. https://doi.org/10.1016/j.renene.2019.05.041.

Fu, Z., et al., 2021. Experimental investigation on the enhanced performance of a solar PVT system using micro-encapsulated PCMs (Aug). Energy vol. 228, 120509. https://doi.org/10.1016/j.energy.2021.120509.

Haloui, H., Touafek, K., Khelifa, A., 2022. Modeling of a hybrid thermal photovoltaic (PVT) collector based on thin film organic solar cells (Sep). Electr. Power Syst. Res. vol. 210, 108131. https://doi.org/10.1016/j.epsr.2022.108131.

Hossain, M.S., Kumar, L., Arshad, A., Selvaraj, J., Pandey, A.K., Rahim, N.A., 2023b. A comparative investigation on solar PVT- and PVT-PCM-based collector constancy performance (Feb). Energies vol. 16 (5), 2224. https://doi.org/10.3390/en16052224.

Hossain, M.S., Kumar, L., Arshad, A., Selvaraj, J., Pandey, A.K., Rahim, N.A., 2023a. A comparative investigation on Solar PVT- and PVT-PCM-based collector constancy performance. Energies vol. 16 (5). https://doi.org/10.3390/en16052224.

Kabeel, A.E., Khalil, A., Shalaby, S.M., Zayed, M.E., 2017. Improvement of thermal performance of the finned plate solar air heater by using latent heat thermal storage (Aug). Appl. Therm. Eng. vol. 123, 546–553. https://doi.org/10.1016/j.applthermaleng.2017.05.126.

Kalidasan, B., Pandey, A.K., Shahabuddin, S., Samykano, M., Thirugnanasambandam, M., Saidur, R., 2020. Phase change materials integrated solar thermal energy systems: global trends and current practices in experimental approaches. J. Energy Storage vol. 27 (November 2019), 101118. https://doi.org/10.1016/j.est.2019.101118.

Kanka, S.D., et al., 2024. Impact of various environmental parameters and production enhancement techniques on direct solar still: a review (Jan). Sol. Energy vol. 267, 112216. https://doi.org/10.1016/j.solener.2023.112216.

Kibria, Md.G., Mohtasim, Md.S., Paul, U.K., Das, B.K., Saidur, R., 2024b. Impact of hybrid nano PCM (paraffin wax with Al2O3 and ZnO nanoparticles) on photovoltaic thermal system: energy, exergy, exergoeconomic and enviroeconomic analysis (Jan). J. Clean. Prod. vol. 436, 140577. https://doi.org/10.1016/j.jclepro.2024.140577.

Kibria, Md.G., Paul, U.K., Mohtasim, Md.S., Das, B.K., Mustafi, N.N., 2024a. Characterization, optimization, and performance evaluation of PCM with Al2O3 and ZnO hybrid nanoparticles for photovoltaic thermal energy storage (Jun). Energy Built Environ.. https://doi.org/10.1016/j.enbenv.2024.06.001.

Koca, A., Oztop, H.F., Koyun, T., Varol, Y., 2008. Energy and exergy analysis of a latent heat storage system with phase change material for a solar collector (Apr). Renew. Energy vol. 33 (4), 567–574. https://doi.org/10.1016/j.renene.2007.03.012.

Li, J., et al., 2022. A hybrid photovoltaic and water/air based thermal(PVT) solar energy collector with integrated PCM for building application (Nov). Renew. Energy vol. 199, 662–671. https://doi.org/10.1016/j.renene.2022.09.015.

Liu, Z., Wang, Z., Ma, C., 2006. An experimental study on heat transfer characteristics of heat pipe heat exchanger with latent heat storage. Part I: charging only and discharging only modes. Energy Convers. Manag. vol. 47 (7–8), 944–966. https://doi.org/10.1016/j.enconman.2005.06.004.

H. Mey, "Carbon black: Enhancing phase change materials for direct solar application," pp. 2016–2027, 2016.

Mohd Razali, N.F., Fudholi, A., Ruslan, M.H., Sopian, K., 2020. Electrical characteristics of photovoltaic thermal collector with water–titania nanofluid flow (Jul). J. Adv. Res. Fluid Mech. Therm. Sci. vol. 73 (2), 20–28. https://doi.org/10.37934/arfmts.73.2.2028.

Mohtasim, Md.S., Das, B.K., 2024. Biomimetic and bio-derived composite Phase Change Materials for Thermal Energy Storage applications: a thorough analysis and future research directions (Apr). J. Energy Storage vol. 84, 110945. https://doi.org/10.1016/j.est.2024.110945.

Nižetić, S., Jurčević, M., Čoko, D., Arıcı, M., Hoang, A.T., 2021. Implementation of phase change materials for thermal regulation of photovoltaic thermal systems: comprehensive analysis of design approaches (Aug). Energy vol. 228, 120546. https://doi.org/10.1016/j.energy.2021.120546.

V.R. Pawar, M.K. Siddiki, and S. Sobhansarbandi, "Numerical Analysis of a Photovoltaic-Thermal Solar Collector With PCM Embedded in Highly Conductive Porous Material," Jun. 2021. doi: 10.1115/HT2021-62974.

Pierson, H.O., 1993. Preface. Handbook of Carbon Graphite Diamonds and Fullerenes. Elsevier, pp. viii–ix. https://doi.org/10.1016/B978-0-8155-1339-1.50005-0.

Qenawy, M., El-Mesery, H.S., Wang, J., Abdelhady, S., 2023. Design and thermal performance analysis of concentrating solar power tower for water heating systems. Case Stud. Therm. Eng. vol. 48, 103141 https://doi.org/10.1016/j.csite.2023.103141.

Rejeb, O., et al., 2020. Novel solar PV/Thermal collector design for the enhancement of thermal and electrical performances (Feb). Renew. Energy vol. 146, 610–627. https://doi.org/10.1016/j.renene.2019.06.158.

Sari, A., Kaygusuz, K., 2001. Thermal energy storage system using stearic acid as a phase change material (Dec). Sol. Energy vol. 71 (6), 365–376. https://doi.org/10.1016/S0038-092X(01)00075-5.

Siala, F.M., Elayeb, M., 2001. Mathematical formulation of a graphical method for a no-blocking heliostat field layout (May). Renew. Energy vol. 23 (1), 77–92. https://doi.org/10.1016/S0960-1481(00)00159-2.

A.P. Singh, S. Tiwari, R.K. Sahdev, Harender, and P. Tiwari, "Effect of transmissivity on PV module glass for PVT-TEC air collector," in *2022 International Conference on Computational Modelling, Simulation and Optimization (ICCMSO)*, Dec. 2022, pp. 401–406. doi: 10.1109/ICCMSO58359.2022.00083.

Yang, X., Sun, L., Yuan, Y., Zhao, X., Cao, X., 2018. Experimental investigation on performance comparison of PV/T-PCM system and PV/T system (Apr). Renew. Energy vol. 119, 152–159. https://doi.org/10.1016/j.renene.2017.11.094.

Yuan, H., et al., 2022. Fabrication and properties of nanoencapsulated stearic acid phase change materials with Ag shell for solar energy storage (Jun). Sol. Energy Mater. Sol. Cells vol. 239, 111653. https://doi.org/10.1016/j.solmat.2022.111653.

Zarei, A., Elahi, S., Pahangeh, H., 2022. Design and analysis of a novel solar compression-ejector cooling system with eco-friendly refrigerants using hybrid photovoltaic thermal (PVT) collector (Jul). Therm. Sci. Eng. Prog. vol. 32, 101311. https://doi.org/10.1016/j.tsep.2022.101311.

Zhang, Z., Fang, X., 2006. Study on paraffin/expanded graphite composite phase change thermal energy storage material (Feb). Energy Convers. Manag. vol. 47 (3), 303–310. https://doi.org/10.1016/j.enconman.2005.03.004.